Journal of Petroleum Science and Engineering 184 (2020) 106525

Contents lists available at ScienceDirect

Journal of Petroleum Science and Engineering

journal homepage: http://www.elsevier.com/locate/petrol

Enhancing total fracture surface area in naturally fractured unconventional reservoirs via model predictive control

Prashanth Siddhamshetty [a,b], Parth Bhandakkar [a,b], Joseph Sang-Il Kwon [a,b,*]

[a] Artie McFerrin Department of Chemical Engineering, Texas A&M University, College Station, TX 77845, USA
[b] Texas A&M Energy Institute, Texas A&M University, College Station, TX 77845, USA

ARTICLE INFO

Keywords:
Natural fractures
Hydraulic fracturing
Model predictive control
Unconventional reservoirs

ABSTRACT

In naturally fractured unconventional reservoirs, naturally present fractures will interact with hydraulic fractures, and divert fracture propagation. Because of complex fracture growth, the ultimate goal of hydraulic fracturing operation in naturally fractured unconventional reservoirs should be changed from achieving the desired fracture geometry to maximizing the total fracture surface area (TFSA) for given fracturing resources, as it will allow more drainage area available for oil recovery. Unfortunately, there are no such techniques available to develop pumping schedules to maximize TFSA for given fracturing resources in naturally fractured unconventional reservoirs. Motivated by this, in this work, we will develop a new model-based pumping schedule by utilizing a recently developed unconventional complex fracture propagation model called Mangrove as our virtual experiment describing complex fracture networks by accounting for the interaction between hydraulic fractures and natural fractures. Initially, using the simulation data from Mangrove, a reduced-order model (ROM) is constructed, which is then used to develop a Kalman filter utilizing the available measurement to estimate the unmeasurable ROM states. Then, we propose a model-based feedback control system to determine the fracturing fluid pumping schedule that maximizes TFSA, which will lead to an enhanced oil production rate from naturally fractured unconventional reservoirs. We demonstrate that by using the proposed control scheme, TFSA can be greatly enhanced which will lead to an oil production rate greater than those of existing pumping schedules which were developed without considering natural fractures.

1. Introduction

Natural fractures (discontinuities in shale rock formations) are commonly observed in most of the unconventional reservoirs using advanced fracture diagnostic techniques such as microseismic monitoring, core samples and outcrops (Maxwell et al., 2002; Daniels et al., 2007; Gale et al., 2007, 2014). These natural fractures will interact with hydraulic fractures, divert fracture propagation and result in a complex fracture geometry (Dahi-Taleghani and Olson, 2013; Yang et al., 2016). The resulting complex fracture geometry in naturally fractured unconventional reservoirs plays a major role in recovering oil, subsequently determining the performance of the well. Therefore, it is very important to consider the interaction between hydraulic fractures and natural fractures to optimize hydraulic fracturing treatments in naturally fractured unconventional reservoirs.

The three possible scenarios when a propagating hydraulic fracture interacts with a natural fracture are shown in Fig. 1 (Dahi-Taleghani and Olson, 2013). First, the hydraulic fracture will continue to propagate like a planar fracture in the same direction by crossing the natural fracture (Fig. 1a). Second, the hydraulic fracture will divert into the natural fracture and will re-initiate its propagation at the natural fracture's tip (Fig. 1b). Third, the diverted hydraulic fracture will re-initiate at some weak point along the natural fracture (Fig. 1c).

The interaction between hydraulic fractures and natural fractures has been studied experimentally and numerically by many researchers (Blanton, 1986; Warpinski and Teufel, 1987; Renshaw and Pollard, 1995; Dahi-Taleghani and Olson, 2009; Wang et al., 2013). To analyze complex fracture networks, the wire-mesh model (Xu et al., 2009, 2010) and the discrete-fracture-network model (Meyer and Bazan, 2011) are generally used, in which a complex fracture geometry is approximated by the orthogonal grid pattern of hydraulic fractures. However, these approaches ignore the mechanism of how natural and hydraulic fractures interact. Olson and Taleghani (2009) developed a model to describe multiple, nonplanar, pseudo-3-dimensional (P3D) fracture

* Corresponding author. Artie McFerrin Department of Chemical Engineering, Texas A&M University, College Station, TX 77845, USA.
E-mail address: kwonx075@tamu.edu (J.S.-I. Kwon).

https://doi.org/10.1016/j.petrol.2019.106525
Received 2 July 2019; Received in revised form 10 September 2019; Accepted 23 September 2019
Available online 27 September 2019
0920-4105/Published by Elsevier B.V.

propagation in naturally fractured unconventional reservoirs, but the model did not consider pressure drops in fractures due to fluid flow. Budyn et al. (2004) and Keshavarzi et al. (2012) modeled the hydraulic fracture propagation using an extended-finite-element-method (XFEM) model to analyze the natural and hydraulic fracture interaction. However, both of these XFEM models are two-dimensional (2D) and do not consider the three-dimensional (3D) effects such as the evolution of fracture height. Recently, Wu and Olson (2014) developed a complex hydraulic fracturing model by employing the 3D displacement discontinuity method, which was computationally efficient. In this model, the hydraulic fracture propagation direction during its interaction with natural fractures was determined using a crossing criterion by modifying the extended Renshaw and Pollard criterian (Renshaw and Pollard, 1995; Gu and Weng, 2010). However, this model did not consider the proppant transport in naturally fractured unconventional reservoirs. Recently, Weng et al. (2014) developed an unconventional fracture model (UFM) by considering height growth, fracture deformation, fluid flow and proppant transport in naturally fractured unconventional reservoirs to simulate complex fracture network. Based on the UFM, Schlumberger developed a hydraulic fracture simulator called Mangrove which is an engineered stimulation package available in Schlumberger Petrel platform. In this work, we have used Mangrove as a virtual experiment to simulate the complex fracture growth in naturally fractured unconventional reservoirs.

In hydraulic fracturing, achieving an optimal fracture geometry is important as it will maximize the oil production rate from unconventional reservoirs (Siddhamshetty et al., 2017). Recently, several studies have been conducted to compute the fracturing fluid pumping schedule by developing real-time model-based feedback control strategies and to achieve an optimal fracture geometry (Gu and Hoo, 2014; Narasingam et al., 2017, 2018; Sidhu et al., 2018a, b; Yang et al., 2017; Siddhamshetty et al., 2017, 2018a, 2018b, 2019; Siddhamshetty and Kwon, 2019). However, they did not consider natural fractures, which may result in a complex fracture geometry. Because of this complex fracture growth behavior, the ultimate goal of hydraulic fracturing in naturally fractured unconventional reservoirs should be changed from achieving the desired fracture geometry to maximizing the total fracture surface area (TFSA) for given fracturing resources such as water, proppant, viscosifying agent, etc. This will increase the drainage area, thereby enhancing the overall oil production rate in naturally fractured unconventional reservoirs (Wu and Olson, 2016). Therefore, the pumping schedule computed using existing control schemes cannot be directly applied to naturally fractured unconventional reservoirs. Motivated by this, in this work, we develop a model-based pumping schedule to maximize TFSA by utilizing Mangrove to describe complex fracture growth in naturally fractured unconventional reservoirs.

This paper is organized as follows: High-fidelity model formulation using Mangrove is described in Section 2. In Section 3, we present a sensitivity analysis to show the importance of maximizing TFSA in naturally fractured unconventional reservoirs. In Section 4, we present existing pumping schedule design techniques and their drawbacks. In Section 5, we construct a reduced-order model (ROM) that describes the relationship between the manipulated input variables (i.e., flow rate of fracturing fluid and proppant concentration at the wellbore) and output variable (i.e., TFSA) using the data generated from Mangrove. Next, we design a Kalman filter utilizing the available measurement to estimate the unmeasurable ROM states. In Section 6, we present a model-based feedback control framework to compute the fracturing fluid pumping schedule that maximizes TFSA with given resources. In Section 7, we present the closed-loop simulation results to demonstrate that the obtained TFSA can lead to an enhanced oil production rate from naturally fractured unconventional reservoirs.

2. High-fidelity model formulation using Mangrove

In this section, we will discuss the UFM developed by Weng et al. (2014), which considers the complex fracture growth in naturally fractured unconventional reservoirs.

2.1. Overview of the UFM

The UFM introduced by Weng et al. (2014) has assumptions and equations very similar to that of P3D model, but solves a problem where fluid flow and rock deformation are coupled in a complex fracture network. A key advantage of the UFM is that it is able to simulate the interaction of hydraulic fractures with pre-existing natural fractures. In particular, it determines whether (a) a hydraulic fracture propagates like a planar fracture in the same direction by crossing a natural fracture, (b) a hydraulic fracture is arrested when it interacts with a natural fracture, or (c) a hydraulic fracture diverts into a natural fracture and subsequently propagates along a natural fracture. In addition to the interaction between hydraulic fractures and natural fractures, the UFM also considers the interaction between adjacent fractures (i.e., the stress-shadow effect). The UFM solves a system of governing equations describing fluid flow in the fracture network, mass conversation, fracture deformation, height growth, proppant transport and fracture interaction to simulate the propagation of a complex fracture network that consists of many intersecting fractures, which are described below.

2.1.1. Fluid flow equations

The local mass conservation equation at any location in the complex fracture network is given as:

$$\frac{\partial q}{\partial s}+\frac{\partial\left(H_{fl}\overline{w}\right)}{\partial t}+q_L=0 \tag{1}$$

$$q_L=2h_Lu_L \tag{2}$$

where H_{fl} is the height of a fracture at position s and time t, q denotes the local fracturing fluid flow rate, $\overline{w}$ is the average width of a fracture at position $s=s(x,y)$, and q_L is the leak-off volume rate through the hydraulic fracture wall (leak-off velocity, u_L, times leak-off fracture height, h_L), which is computed using Carter's leak-off model.

The pressure drop along a fracture branch in a complex fracture

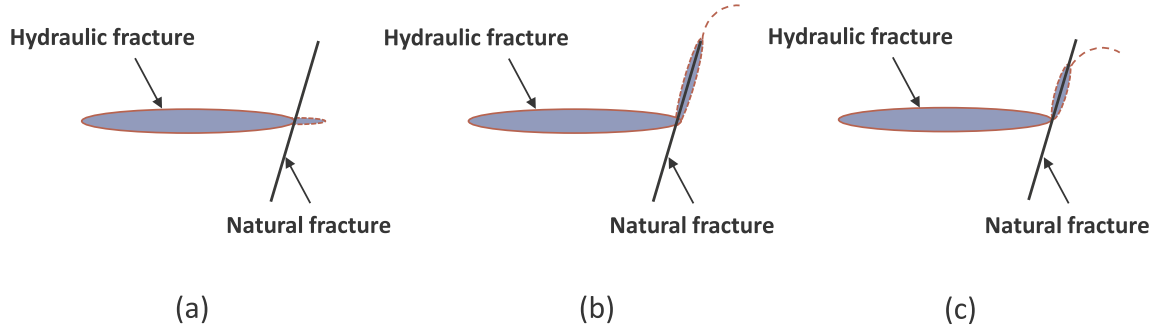

Fig. 1. Possible scenarios when a hydraulic fracture interacts with a natural fracture.

network for laminar flow of power-law fluid can be expressed using Poiseuille law:

$$\frac{\partial p}{\partial s} = -\alpha_0 \frac{1}{\overline{w}^{2n'+1}} \frac{q}{H_{fl}} \left|\frac{q}{H_{fl}}\right|^{n'-1} \tag{3a}$$

and for turbulent fracturing fluid flow:

$$\frac{\partial p}{\partial s} = -\frac{f\rho}{\overline{w}^3} \frac{q}{H_{fl}} \left|\frac{q}{H_{fl}}\right| \tag{3b}$$

where

$$\alpha_0 = \frac{2k'}{\varphi(n')^{n'}} \cdot \left(\frac{4n'+2}{n'}\right)^{n'};\ \varphi(n') = \frac{1}{H_{fl}} \int_{H_{fl}} \left(\frac{w(z)}{\overline{w}}\right)^{\frac{2n'+1}{n'}} dz \tag{4}$$

where p is the fluid pressure, $w(z)$ denotes the fracture width as a function of depth z, f represents the fanning factor, ρ is the density of slurry, and n' and k' are the fracturing fluid power-law index and consistency index, respectively.

The fracture height and width profiles in a multi-layered formation depends on the fluid pressure, fracture toughness, in-situ stresses, layer thickness and elastic modulus of each layer. The fracture height is calculated by matching the fracture toughness to the stress intensity factors at fracture tips. Stress intensity factors K_{1u}, K_{1l} and width profile are given as follows (Mack et al., 1992):

$$K_{1u} = \sqrt{\frac{\pi h}{2}}\left[p_{cp} - \sigma_n + \rho_f g\left(h_{cp} - \frac{3h}{4}\right)\right] + \sqrt{\frac{2}{\pi h}}\sum_{i=1}^{n-1}(\sigma_{i+1} - \sigma_i) \times \left[\frac{h}{2}\arccos\left(\frac{h-2h_i}{h}\right) - \sqrt{h_i(h-h_i)}\right] \tag{5a}$$

$$K_{1l} = \sqrt{\frac{\pi h}{2}}\left[p_{cp} - \sigma_n + \rho_f g\left(h_{cp} - \frac{h}{4}\right)\right] + \sqrt{\frac{2}{\pi h}}\sum_{i=1}^{n-1}(\sigma_{i+1} - \sigma_i) \times \left[\frac{h}{2}\arccos\left(\frac{h-2h_i}{h}\right) + \sqrt{h_i(h-h_i)}\right] \tag{5b}$$

$$w(z) = \frac{4}{E'}\left[p_{cp} - \sigma_n + \rho_f g\left(h_{cp} - \frac{h}{4} - \frac{z}{2}\right)\right]\sqrt{z(h-z)} + \frac{4}{\pi E'}\sum_{i=1}^{n-1}(\sigma_{i+1} - \sigma_i) \left[(h_i - z)\,\mathrm{arcCosh}\frac{z\left(\frac{h-2h_i}{h}\right) + h_i}{|z-h_i|} + \sqrt{z(h-z)}\arccos\left(\frac{h-2h_i}{h}\right)\right] \tag{5c}$$

where K_{1u} and K_{1l} are the stress intensity factors at the top and bottom of fracture tips, respectively, h is the fracture height, p_{cp} is fracturing fluid pressure at height h_{cp} measured from the bottom tip of the reference fracture, σ_n and σ_i are the in-situ stresses at the top and the i^{th} layer, respectively, h_i is the distance between the fracture bottom tip and top of i^{th} layer, ρ_f is the fluid density and $E' = E/(1-\nu^2)$ where E is Young's modulus, ν is Poisson's ratio.

In addition to the above equations, the following global volume balance must be satisfied at each time:

$$\int_0^t Q(t)dt = \int_0^{L(t)} h(s,t)\overline{w}(s,t)ds + \int_{H_L}\int_0^t \int_0^{L(t)} 2u_L ds dt dh_L \tag{6}$$

where t is the current time, $L(t)$ is the total fracture length in the hydraulic fracture network at time t and $Q(t)$ is the fracturing fluid flow rate at the wellbore. The global volume balance equation essentially signifies that the total volume of injected fracturing fluid is equal to the volumes of fracturing fluid present in the fracture network and leak-off fluid to the surrounding formation.

These equations, along with the boundary conditions stating that the fracture tip's width, net pressure and flow rate are zero, describe the fluid flow through a complex fracture network.

2.1.2. Hydraulic and natural fractures interaction

The interaction between propagating hydraulic fractures and pre-existing natural fractures is a very complex phenomenon. The modeling of this system requires consideration of various rock properties like Young's modulus, tensile strength, poisson's ratio, toughness, permeability and cohesion. It should also incorporate various fracturing fluid properties like viscosity, density and pressure. In addition to this, mechanical properties like cluster spacing and relative angle between hydraulic fractures and natural fractures also govern whether a hydraulic fracture will cross a natural fracture, dilate a natural fracture, or be arrested at a natural fracture as explained by Wu and Olson (2016). The average opening width of a fracture (Valko and Economides, 1995) and average pressure of a fracturing fluid in the natural fracture (Chuprakov et al., 2013, 2014) are governed by the following equations:

$$\overline{w} = 2.53\left[\frac{Q\mu L^2}{E'H}\right]^{1/4} \quad p_{NF}(t) = p_f \tanh\left(\sqrt{\frac{2kp_f}{\mu b_s^2}}t\right) \tag{7}$$

where μ is the slurry viscosity, p_f is the fracture tip's fluid pressure, p_{NF} is the fluid pressure within a natural fracture, k is the permeability of natural fracture, t is the contact time and b_s is the boundary of sliding zone as a result of contact between a natural fracture and hydraulic fracture.

2.1.3. Stress shadow effects

Stress shadow effects refer to alteration in the growth pattern of a hydraulic fracture due the presence of neighboring fractures. The disturbance from nearby fractures leads to a significant perturbation in the propagating hydraulic fracture. In this work, 2D Displacement Discontinuity Method (DDM) described by Crouch et al. (1983) is used to quantify the normal and shear stresses on a fracture element due to opening and shearing displacement discontinuities. It is defined as follows:

$$\sigma_n^i = \sum_{j=1}^{N} A^{ij} C_{ns}^{ij} D_s^j + \sum_{j=1}^{N} A^{ij} C_{nn}^{ij} D_n^j \tag{8a}$$

$$\sigma_s^i = \sum_{j=1}^{N} A^{ij} C_{ss}^{ij} D_s^j + \sum_{j=1}^{N} A^{ij} C_{sn}^{ij} D_n^j \tag{8b}$$

where σ_n and σ_s are the normal and shear stresses, respectively, D_n and D_s are the opening and shearing displacement discontinuities, respectively, C^{ij} are the 2D plane-strain elastic influence coefficients and A^{ij} are the 3D correction factors introduced by Olson (2008) to account for the 3D effect caused by finite fracture height.

Based on this UFM, Schlumberger developed a hydraulic fracture simulator called Mangrove which is an engineered stimulation package available in Schlumberger Petrel platform. In this work, we have used Mangrove to simulate complex fracture growth in naturally fractured unconventional reservoirs.

Remark 1. The parameters required to set up the Mangrove simulator for a specific rock formation are reservoir thickness, Young's modulus, Poisson ratio, minimum and maximum horizontal stresses, and natural fracture properties such as length, orientation and spacing between natural fractures. The minimum horizontal stress of rock formation can be obtained from minifrac or extended leak-off test, and maximum horizontal stress is available from wellbore failure image and modeling. Rock properties such as Young's modulus and Poisson ratio can be obtained from well logs. Microseismic measurements can be used to partially predict the distribution of natural fractures by comparing the effective stimulated volume for a given distribution of natural fractures.

2.2. Reservoir simulator

Apart from simulating complex fracture networks, Mangrove can model the oil production through proppant-propped complex fractured networks. Specifically, the output from the UFM is fed as an input to the automated grid generator (Cipolla et al., 2011). After establishing the production grid including a complex fracture geometry, we simulate production from an oil well in a naturally fractured unconventional reservoir using Mangrove. Then the Net Present Value (NPV) of the oil produced from the well is calculated using the following equation:

$$NPV = \int_0^T Q_{oil} r_{oil} (1+I)^{-ct} dt \tag{9}$$

where Q_{oil} is the oil production rate from the well, t is the elapsed time since the oil production was initiated, T is the total oil production time, r_{oil} is the oil market price, c is the time constant, and I is the money discount rate. In this work, c and I are taken as 0.1 and 1/365 (1/day), respectively.

3. Sensitivity analysis of complex fracture growth in naturally fractured reservoirs

During hydraulic fracture propagation in naturally fractured reservoirs, the complex fracture growth depends on in-situ stresses, rock mechanical properties, natural fracture properties and hydraulic fracture treatment parameters (e.g., fracturing fluid properties and pumping schedules). In this section, we performed sensitivity analysis on the effect of natural fracture distribution (e.g., length, orientation and spacing between natural fractures) and fracturing fluid pumping schedule (e.g., flow rate and proppant concentration injected at the wellbore) on TFSA for given rock properties (e.g., Young's modulus, Poisson ratio and in-situ stresses).

3.1. Effect of natural fracture distribution on TFSA

For all the simulations, we considered a single-stage hydraulic fracturing operation with three simultaneously propagating multiple fractures from the three clusters with a fracture spacing of 100 ft. We considered a total of 487200 lb proppant available for injection per stage. All the other parameters used in the simulations are given in Table 1.

3.1.1. Effect of natural fracture orientation on TFSA

The orientation of natural fractures, which is defined by the relative angle (β in Fig. 2) between hydraulic fractures and natural fractures, is one of the important factors affecting the final fracture geometry. As the relative angle decreases, the tendency of hydraulic fractures to cross natural fractures decreases (Gu et al., 2011). Consequently, hydraulic fracture propagation will divert into natural fractures leading to a complex fracture geometry. In this sensitivity analysis, we considered four different relative angles (0°, 30°, 45° and 90°) with a differential stress (i.e., the difference between the maximum and minimum horizontal stresses) of 200 psi and all other parameters were kept as same of those given in Table 1. The total number of natural fractures, their lengths, and inter-fracture spacing were generated assuming they will follow normal distributions (Weng et al., 2011). The statistical parameters used to generate natural fractures with different relative angles are given in Table 2 and the corresponding 2D traces of fracture networks are shown in Fig. 3.

We observed that hydraulic fractures are unable to cross natural fractures for the four relative angles considered in this work. Instead, they diverted into natural fractures leading to a complex fracture geometry as shown in Fig. 3. Mangrove uses the crossing criterion developed by Chuprakov et al. (2014) to predict the interaction between hydraulic fractures and natural fractures; the criterion was developed by considering the effect of in-situ stress ratio, friction coefficient, relative angle, flow rate and viscosity. As per this criterion, a fracturing fluid will leak into natural fractures and divert the hydraulic fracturing propagation when the product of fracturing fluid flow rate, Q, and viscosity, μ, is small (i.e., $Q\mu$ is a small value); otherwise, when the product value is large, hydraulic fractures tend to cross natural fractures and propagate in the same direction, like planar fractures. We considered a slick water for hydraulic fracturing which is of very-low viscosity (0.64 cp), and thus, hydraulic fractures diverted into natural fractures for the four relative angles resulting in a complex fracture geometry (Fig. 3). In addition, TFSA is also affected by the relative angles as shown in Fig. 4. When the relative angle is 0°, hydraulic fractures will propagate in the direction of the maximum horizontal stress after diverting into natural fractures (Fig. 2). In this case, the compressional stress acting perpendicular to the surface of hydraulic fractures is the minimum horizontal stress. As the relative angle increases, the compressional stress acting on hydraulic fractures after diverting into natural fractures increases. Eventually, at 90° the compressional stress acting on hydraulic fractures is the maximum horizontal stress. In summary, the fracture growth becomes more restricted with relative angle (Fig. 3). Therefore, as can be seen from Fig. 4, a smaller relative angle generates a higher TFSA.

Table 1
Model parameters used for sensitivity studies.

Parameter	Value
Fracturing fluid flow rate	60 bbl /min
Stage length	200 ft
Reservoir thickness	500 ft
Young's modulus	1.57 Mpsi
Poisson ratio	0.35
Proppant particle density	2640 kg /m^3
Slick-water density	1000 kg /m^3
Viscosity	0.64 cp
Minimum horizontal stress	4450 psi
Maximum horizontal stress	4650 psi
Perforations in each cluster	12
Diameter of each perforation	0.42 in
Proppant mesh size	80 /100
Diameter of proppant	0.00647 in
Friction coefficient	0.6

3.1.2. Effect of natural fracture length on TFSA

As observed from the data obtained from Barnett shale (Weng et al., 2011), the length of natural fractures in naturally fractured reservoirs is not constant. Generally, natural fractures with different lengths are generated using a normal distribution to replicate the field case. In this sensitivity analysis, we considered two different distributions of natural fracture length as given in Table 3 with a fixed relative angle of 45°. All other parameters were used as described in Table 1. The 2D trace of natural fracture network and final complex fracture network obtained at the end of hydraulic fracturing operation for these two cases are shown in Fig. 5. It is observed that the hydraulic fracture propagation pattern depends on the length of natural fractures. Hydraulic fractures tend to

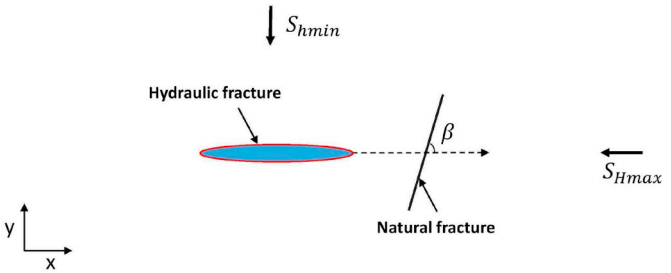

Fig. 2. Schematic showing a hydraulic fracture approaching a natural fracture.

Table 2
Natural fracture distribution with different relative angles.

	Length (ft)	Spacing (ft)	Friction coefficient	Relative angles			
Average	100	50	0.6	0°	30°	45°	90°
Standard deviation	50	5	0	0°	0°	0°	0°

propagate in the direction of natural fractures when the length of natural fractures is long; whereas in the case of short natural fracture length, they tend to propagate in the original hydraulic fracture propagation direction. In addition, TFSA is also affected by natural fractures length, as shown in Fig. 6. Until a hydraulic fracture diverts into a natural fracture, the compressional stress acting perpendicular to the fracture surface area is the minimum horizontal stress. However, after it diverts, the compressional stress becomes greater than the minimum horizontal stress. This happens due to a change in the fracture orientation until the fracture grows out of a natural fracture. For longer natural fracture lengths, the high compressional strength will act for a longer time period which further restricts fracture growth and generates a less TFSA compared to those of shorter natural fracture lengths.

3.1.3. Effect of natural fracture spacing on TFSA

In this sensitivity analysis, we considered two different distributions for natural fracture spacing as given in Table 4 with a fixed relative angle of 45°. All other parameters were kept as described in Table 1. The 2D trace of natural fracture network and final complex fracture network obtained at the end of hydraulic fracturing operation for these two cases are shown in Fig. 7. It is observed that a decrease in natural fracture spacing leads to a more complex fracture geometry, as more natural fractures are likely to be encountered by hydraulic fractures. Because of this complex interaction of hydraulic fractures with multiple closely-spaced natural fractures, TFSA decreases with natural fracturing spacing as shown in Fig. 8.

Based on the sensitivity analysis presented above, we can observe that the natural fracture distribution (e.g., spacing, length and orientation) has a major impact on complex fracture growth during hydraulic fracturing in naturally fractured unconventional reservoirs. Therefore, it is very important to consider the interaction between hydraulic fractures and natural fractures to optimize the hydraulic fracturing treatment in naturally fractured unconventional reservoirs. In practice, microseismic measurements can be used to partially predict the distribution of natural fractures by comparing the effective stimulated volume for a given distribution of natural fractures. In this work, we assume that the natural fracture distribution is available to design a model-based feedback control framework to compute the pumping schedule by maximizing TFSA for given fracturing resources.

3.2. Effect of pumping schedule on TFSA

In this subsection, we performed a sensitivity analysis to find the effect of fracturing fluid pumping schedule (i.e., flow rate and proppant concentration at the wellbore) on TFSA at the end of pumping for given rock properties (e.g., Young's modulus, Poisson ratio and in-situ stresses), natural fracture distribution (length, orientation and spacing between natural fractures) and amount of proppant. The statistical parameters used to generate the natural fracture distribution are given in Table 7. We considered a total amount of $M_{prop} = 487200$ lb proppant to

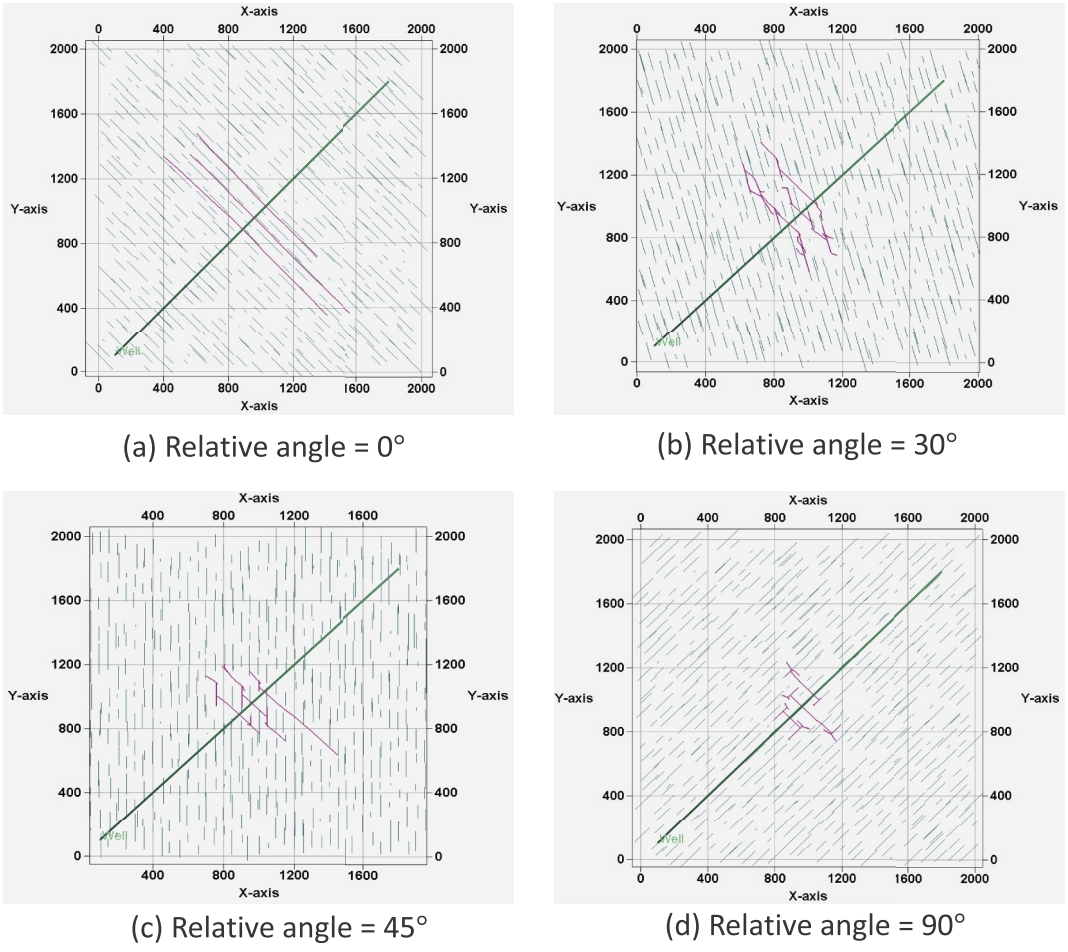

Fig. 3. Fracture network at the end of hydraulic fracturing operation for four different relative angles between hydraulic fractures and natural fractures.

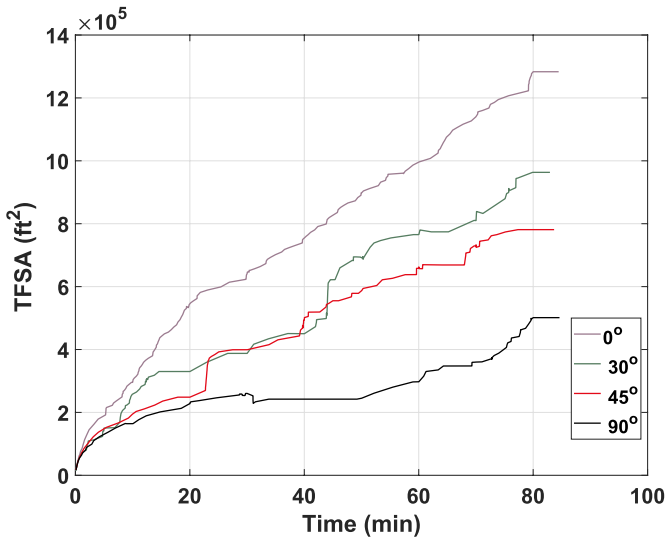

Fig. 4. Comparison of TFSA for four different relative angles between hydraulic fractures and natural fractures.

Table 3
Natural fracture distribution with different lengths.

	Relative angle	Spacing (ft)	Friction coefficient	Length (ft)	
Average	45°	40	0.6	100	200
Standard deviation	0°	5	0	50	50

be injected for creating fractures in a stage. All the other parameters used in the simulations are given in Table 1. We generated three fractures in a single stage with a fixed fracture spacing. For the purpose of sensitivity studies, we considered three cases with three different pumping schedules. The pumping schedule used in each case and the evolution of TFSA with time are shown in Fig. 9 and Fig. 10, respectively. We can clearly see that TFSA depends on pumping schedules.

Thereafter, we simulated the corresponding oil production for 30 years in each case using the reservoir properties given in Table 5 and the generated complex fracture geometry at the end of hydraulic fracturing operation. The cumulative oil production is shown in Fig. 11, where it can be observed that the oil production rate is proportional to TFSA at the end of pumping. This can also be seen from the results presented in Table 6, where it is observed that a reduction of 18% in TFSA at the end of pumping leads to a reduction of around 60% in the cumulative oil production at the end of 30 years. This is mainly due to the fact that the drainage area for hydrocarbon recovery is directly related to TFSA, and achieving a greater TFSA will lead to a greater oil production rate in naturally fractured unconventional reservoirs. Therefore, because of complex fracture growth, the main goal of hydraulic fracturing in naturally fractured unconventional reservoirs should be to maximize TFSA by manipulating the fracturing fluid pumping schedule for given resources as it will lead to more oil recovery.

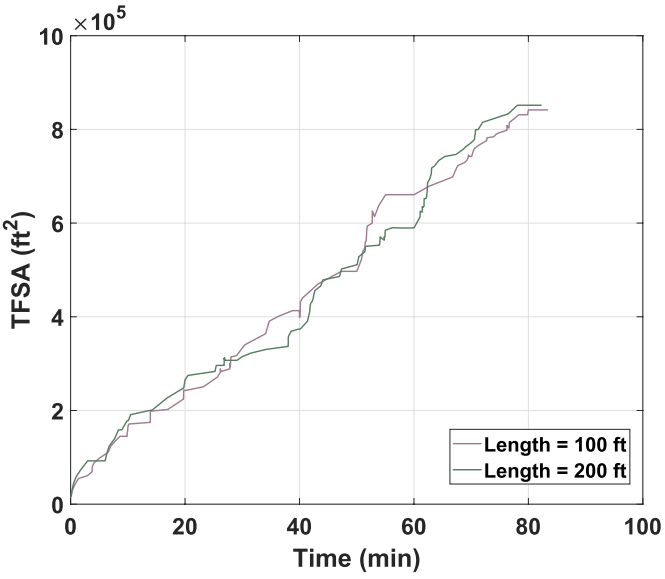

Fig. 6. Comparison of TFSA for two different natural fracture length distributions.

Table 4
Natural fracture distribution with different spacing values.

	Relative angle	Length (ft)	Friction coefficient	Spacing (ft)	
Average	45°	100	0.6	20	60
Standard deviation	0°	50	0	5	5

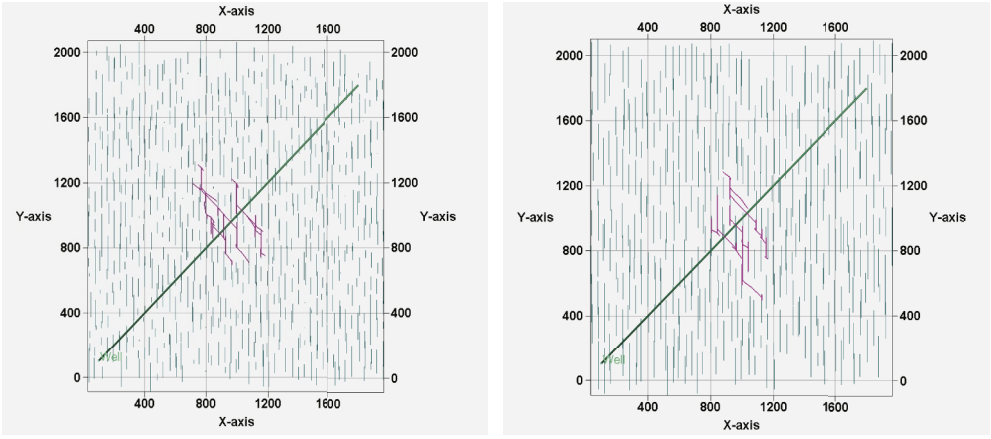

(a) Average length = 100 ft (b) Average length = 200 ft

Fig. 5. Fracture network at the end of hydraulic fracturing operation for two different natural fracture length distributions.

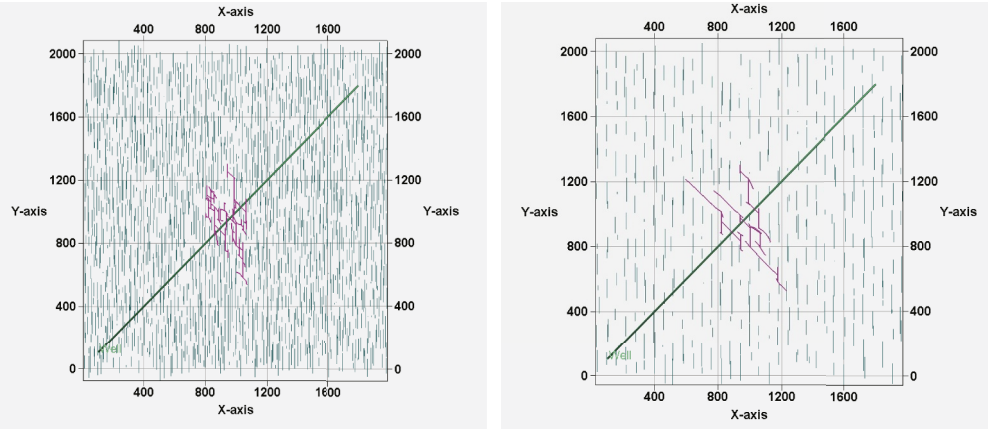

Fig. 7. Fracture network at the end of hydraulic fracturing operation for two different natural fracture spacing distributions.

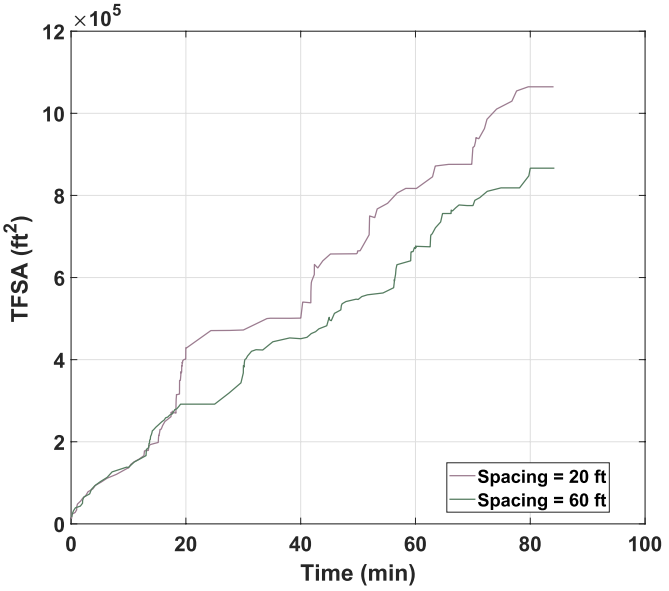

Fig. 8. Comparison of TFSA for two different natural fracture spacing distributions.

4. Background on pumping schedule design techniques

In this section, we present currently available pumping schedule design techniques. Nolte (1986) developed a power-law type proppant concentration schedule, $C_0(t)$, which is given below:

$$C_0(t) = \begin{cases} C_{target}\left(\dfrac{t-t_p}{t_e-t_p}\right)^{\varepsilon} & \text{for } t \geq t_p \\ 0 & \text{for } t < t_p \end{cases} \tag{10}$$

where the desired proppant concentration at the end of hydraulic fracturing operation is denoted using C_{target}, ε is an exponent which depends on fracturing fluid efficiency η, the total time for pumping is denoted using t_e, and $t_p = \varepsilon t_e$ is the pad time at which injection of proppant is started. Because of its easy-to-implement nature, Nolte's pumping schedule has been widely used, however it has the following practical limitations: (1) both proppant settling due to gravity and practical constraints are not considered; (2) because of the predefined form if there is a plant-model mismatch, it will lead to early termination of hydraulic fracturing by creating a shorter propped fracture length; (3) the pumping schedule is designed offline and applied in an open-loop manner to a hydraulic fracturing process; (4) focused only on a single hydraulic fracture; and (5) interaction between hydraulic fractures and natural fractures is not considered.

Recently, to overcome the limitations of Nolte's pumping schedule, a new model-based control system was developed to compute fracturing fluid pumping schedules online to achieve a uniform proppant distribution and optimal fracture geometry in simultaneously growing multiple fractures (Siddhamshetty et al., 2019). Specifically, they considered a dynamic model of simultaneously propagating multiple fractures including fracture propagation, stress shadow effect and proppant transport. However, they did not consider the interaction between hydraulic fractures and natural fractures, which resulted in fractures with a planar shape.

As shown from the sensitivity analysis presented in Section 3, hydraulic fracturing operation in naturally fractured unconventional reservoirs may result in a complex fracture geometry and it is very important to maximize TFSA at the end of pumping as it is directly related to oil production rate. Pumping schedule design techniques mentioned above, which were developed to achieve a specific fracture geometry (length, width and height), may not result in the maximum TFSA when directly applied to naturally fractured unconventional reservoirs. Therefore, in the following section, a model predictive controller (MPC) is developed to compute the pumping schedule that will maximize TFSA in naturally fractured unconventional reservoirs by utilizing Mangrove, which will eventually lead to an enhanced oil production rate.

5. Handling computational requirement in control of hydraulic fracturing processes

The UFM described using Eqs. (1)–(8) is computationally very expensive to be used directly for the design of MPC. In this work, we developed a ROM using MOESP algorithm to describe hydraulic fracture propagation and proppant transport phenomena in naturally fractured unconventional reservoirs, which is given below:

$$x(t_{k+1}) = Ax(t_k) + Bu(t_k) \tag{11a}$$

$$y(t_k) = Cx(t_k) \tag{11b}$$

where $u(t_k) = [Q_{x0}(t_k), C_0(t_k)]^{\mathrm{T}}$ are the input variables, $Q_{x0}(t_k)$ and $C_0(t_k)$ are the fracturing fluid flow rate and proppant concentration injected at the wellbore, respectively, the output variable, $y(t_k) = [A_{frac}(t_k)]$ is TFSA, and the ROM states are represented using $x(t_k)$. For a system with a given order, the model parameters to be determined include the

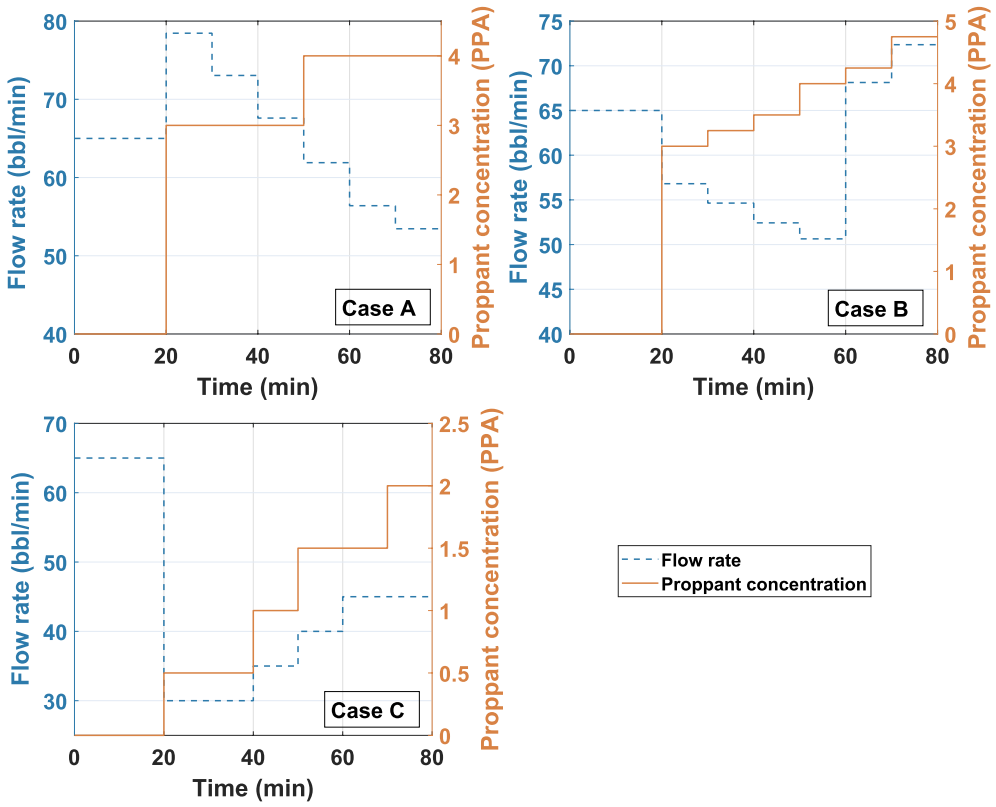

Fig. 9. Pumping Schedules used for sensitivity analysis.

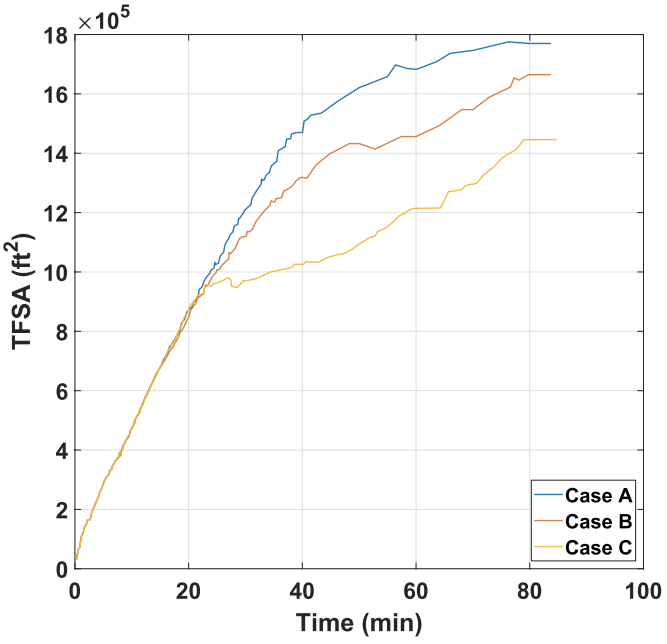

Fig. 10. Comparison of TFSA for three cases with different pumping schedules.

matrices A, B, and C, and the initial state estimate, $x(0)$, using a training data set.

For training, we used an open-loop simulation data obtained using Mangrove to obtain a 2^{nd} order linear time-invariant state-space model. The training input is chosen by considering the minimum and maximum allowable fracturing flow rate and proppant concentration. Fig. 12 shows the comparison between the estimated and true TFSA with time.

Table 5
Reservoir properties used for the oil production simulation.

Parameters	Value
Reservoir rock type	Consolidated sandstone
Permeability	0.0001 – 0.0005mD
Porosity	0.08
Reservoir pressure	5000 psi
Unpropped fracture conductivity	10^{-3}mD.ft
Production time	30 years

It is observed that the estimated TFSA from the ROM quickly converges to the true value obtained from the high-fidelity process model. The computational requirement to solve Eq. (11) is a small fraction relative to that of solving the UFM, Eqs. (1)–(8). We have validated the ROM by comparing its performance with the high fidelity model by considering a different pumping schedule within the limits of minimum and maximum fracturing flow rate and proppant concentration considered while developing the ROM. Fig. 13 shows that TFSA obtained from the ROM is close to the high fidelity model.

In the present work, we assumed that TFSA is measurable, which is then used for estimation of the ROM's states at time $t = t_k$, $x(t_k)$, using a Kalman filter, which is given in the following form:

$$\hat{x}(t_{k+1}) = A\hat{x}(t_k) + Bu(t_k) + M(t_k)(y_m(t_k) - \hat{y}(t_k)) \tag{12a}$$

$$M(t_k) = P(t_k)C^T\left(R(t_k) + CP(t_k)C^T\right)^{-1} \tag{12b}$$

$$P(t_{k+1}) = (I - M(t_k)C)P(t_k) \tag{12c}$$

where the variables estimated by the Kalman filter are denoted using $\widehat{(\cdot)}$, $y_m(t_k) = [A_{frac}(t_k)]$ is TFSA, the process and measurement noise covariance matrices are denoted using Q and R, respectively, $M(t_k)$ is the gain

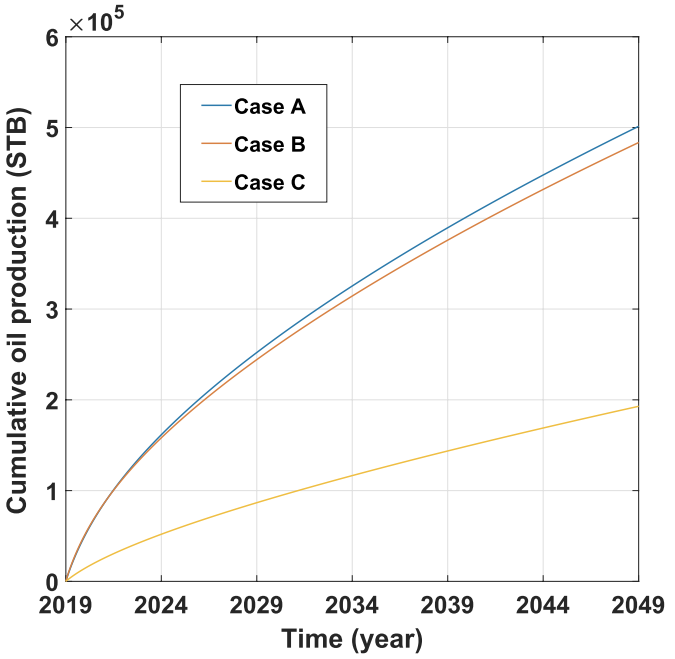

Fig. 11. Cumulative oil production over time for three cases with different pumping schedules.

Table 6
TFSA and cumulative oil production for three cases with different pumping schedules.

Case	TFSA (ft^2)	% Change in TFSA compared to case A	Cumulative oil production (STB)	% Change in production compared to case A
Case A	1769942	0	501542	0
Case B	1664617	- 5.9	483678	- 3.6
Case C	1445647	- 18.3	192969	- 61.5

of Kalman filter, and $P(t_k)$ denotes the state estimation error covariance. In this work, a Kalman filter is used for state estimation. However, other state estimators such as Luenberger observer or moving horizon estimator can be readily used.

Remark 2. In this work, Kalman filter is used to estimate the ROM's states which will also handle any plant-model mismatch by considering the real-time measurement of TFSA. Furthermore, due to the nature of closed-loop operation based on the proposed controller design technique, model-plant mismatch would be handled.

Remark 3. Please note that it is not practical to measure TFSA in real-time. However, TFSA can be estimated from other available measurements using state estimators such as Kalman filter or moving horizon estimator. In practice, we have very limited access to real-time measurements such as the fracture width at the wellbore. Real-time measurement of fracture width at the wellbore can be obtained using the wellbore pressure data and the elasticity equation relating the fracture width at the wellbore and the wellbore pressure (Sukkar and Cornell, 1955; Warpinski et al., 2006; Gu and Hoo, 2014, 2015; Scott et al., 2015; Sun et al., 2016). Previously, we have used this available measurement to estimate unmeasurable variables such as proppant concentration across the fracture and average fracture width using a Kalman filter (Siddhamshetty et al., 2017, 2018a, b). Similarly, we can estimate TFSA by using a Kalman filter and the available real-time measurement of fracture width at the wellbore.

6. Model-based feedback control system for enhancing TFSA in naturally fractured unconventional reservoirs

This section presents a MPC formulation to compute the optimal pumping schedule that maximizes TFSA in naturally fractured unconventional reservoirs at the end of hydraulic fracturing process. The following MPC optimization problem is solved utilizing the ROM and Kalman filter to compute the optimal pumping schedule:

$$\max_{\substack{C_{stage,k},\ldots,C_{stage,8}\\ Q_{stage,k},\ldots,Q_{stage,8}}} \quad A_{frac}(t_f) \tag{13a}$$

$$\text{s.t.} \quad y_m(t_k) = A_{frac}(t_k) \tag{13b}$$

$$\text{ROM, Eq. (11)} \tag{13c}$$

$$\text{Kalman filter, Eq. (12)} \tag{13d}$$

$$C_{stage,k-1+m} \leq C_{stage,k+m} \leq 5 \text{ PPA} \tag{13e}$$

$$Q_{min} \leq Q_{stage,k+m} \leq Q_{max} \tag{13f}$$

$$m = 1, \ldots, 8-k \tag{13g}$$

$$\Delta\left(\sum_{k=1}^{8} Q_{stage,k} C_{stage,k}\right) = M_{prop} \tag{13h}$$

where the duration of each sampling is given by Δ, t_k is the time of k^{th} sample, $y_m(t_k)$ is TFSA measured at $t = t_k$, t_f is the hydraulic fracturing total operation time, and the manipulated input variables, $C_{stage,k}$ and $Q_{stage,k}$, are obtained by solving Eq. (13) with a shrinking prediction horizon $N_p = t_f - t_k$.

In the optimization problem of Eq. (13), a Kalman filter, Eq. (13d), is used to estimate the unmeasurable ROM states and it is initialized at every sampling time utilizing TFSA measured in real-time, which is described by Eq. (13b). Eqs. (13e) and (13f) are the constraints on the manipulated input variables (e.g., proppant concentration and fracturing fluid flow rate injected at the wellbore). The units of fracturing fluid flow rate and proppant concentration are bbl /min and PPA (1 pound of the proppant added to one gallon of fracturing fluid), respectively. The total amount of proppant injected is constrained using Eq. (13h).

7. Closed-loop simulation results under the proposed MPC

In this section, we present the closed-loop simulation results to signify the performance of our proposed MPC scheme. For all the cases, we considered a single stage hydraulic fracturing operation to generate three simultaneously propagating fractures for a given natural fracture distribution. The statistical parameters used to generate the natural fracture distribution are given in Table 7 and the generated natural fracture distribution is shown in Fig. 14. The total proppant amount considered is $M_{prop} = 487200$ lb. All the other parameters used in the simulations are given in Table 1. The high fidelity model of Mangrove described in Section 2 was utilized to simulate a hydraulic fracturing operation in naturally fractured unconventional reservoirs. This model is initially used with a given training input for generating the input/output data which was used to develop the ROM of the process. We then designed a Kalman filter for state estimation using this ROM, which eventually helped us in developing the complete MPC scheme. The Kalman filter and the proposed MPC were initialized at the beginning of hydraulic fracturing operation. In the proposed MPC, Δ and t_f values were chosen to be 10 min and 80 min, respectively. This implies that the fracturing fluid pumping schedule consists of 8 stages, each with a duration of 10 min. We assumed that the measurement of TFSA, $A_{frac}(t_k)$, was available at the beginning of each pumping stage (Eq. (13b)). The

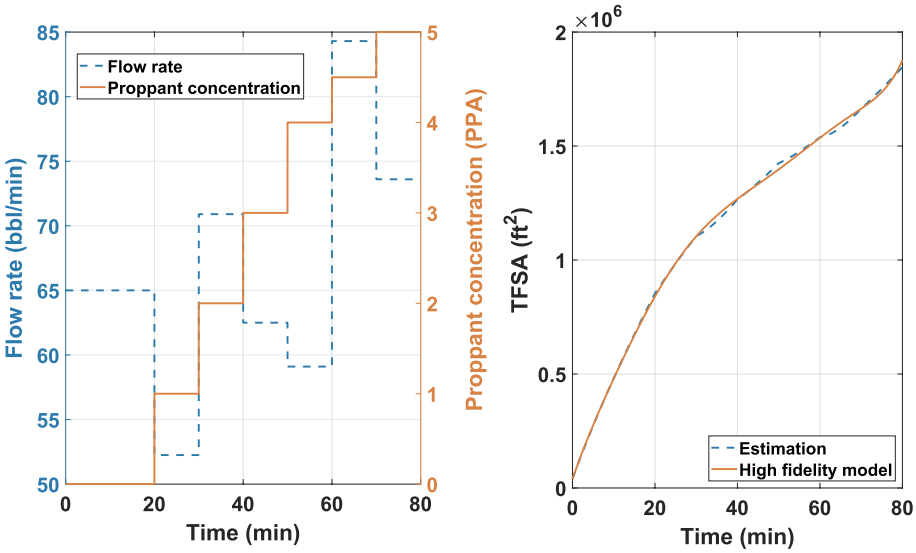

Fig. 12. Comparison between the true values and the estimates of TFSA for a given pumping schedule.

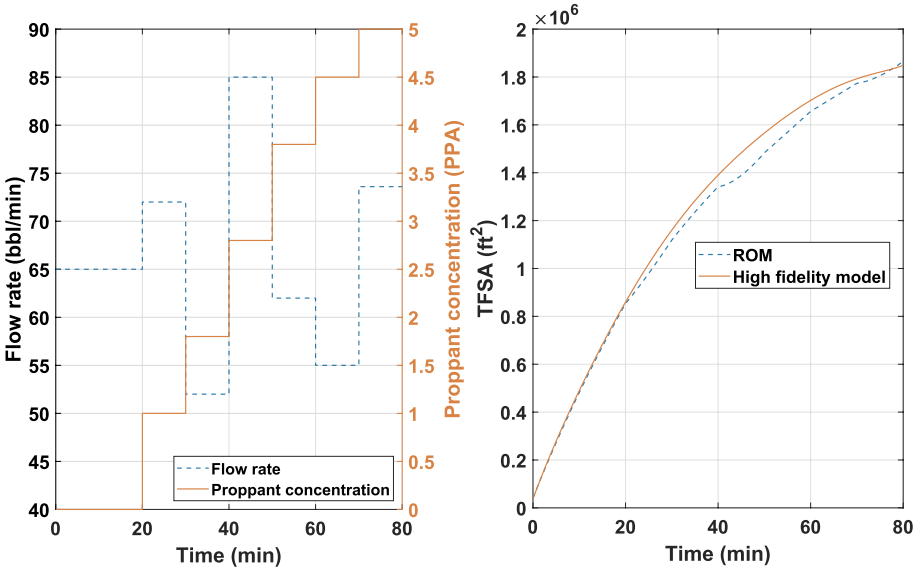

Fig. 13. Validation of the ROM by comparing it with high fidelity model for a given pumping schedule.

unmeasurable ROM's states were then predicted with the help of real-time measurement via the Kalman filter. Using these estimated states, the proposed MPC computed the control input over a prediction horizon length of N_p to maximize TFSA at the end of hydraulic fracturing operation, which will lead to an enhanced oil production rate due to a higher drainage area available for hydrocarbon recovery. We applied the first step of solution, $C_{stage,k}$ & $Q_{stage,k}$, to the high-fidelity model of Mangrove in a sample-and-hold fashion and this procedure was repeated at every sampling time until the end of the process.

The pumping schedule obtained under the proposed MPC scheme (Fig. 15) is then fed as the input to Mangrove. The obtained fracture geometry at the end of hydraulic fracturing operation under the proposed MPC is presented in Fig. 14. For given rock properties and natural fracture distribution, hydraulic fractures divert into natural fractures resulting in a complex fracture geometry. We then compared the performance of the pumping schedule computed by the proposed MPC with the existing pumping schedules such as Nolte (Fig. 16) and the one introduced by Siddhamshetty et al. (2019) (Fig. 17), which were developed without considering natural fractures. All the other parameters such as Young's modulus, Poisson ratio, and proppant amount are kept same in all the cases. Fig. 18 compares the evolution of TFSA for the three cases. Figs. 19 and 20 show the comparison of the cumulative oil production and oil production rates for the three cases. We can see clearly from the figures that the pumping schedule under the proposed MPC maximizes TFSA, which subsequently leads to the maximum oil production rate and maximum cumulative oil production compared to other pumping schedules. We reported the NPV of oil produced for these three cases in Table 8. Using the proposed MPC will result in a revenue that is 0.74 millions and 0.4 millions more than those

Table 7
Natural fracture distribution used in the closed-loop simulation.

	Length (ft)	Spacing (ft)	Orientation	Friction coefficient
Average	500	100	15	0.5
Standard deviation	250	50	15	0

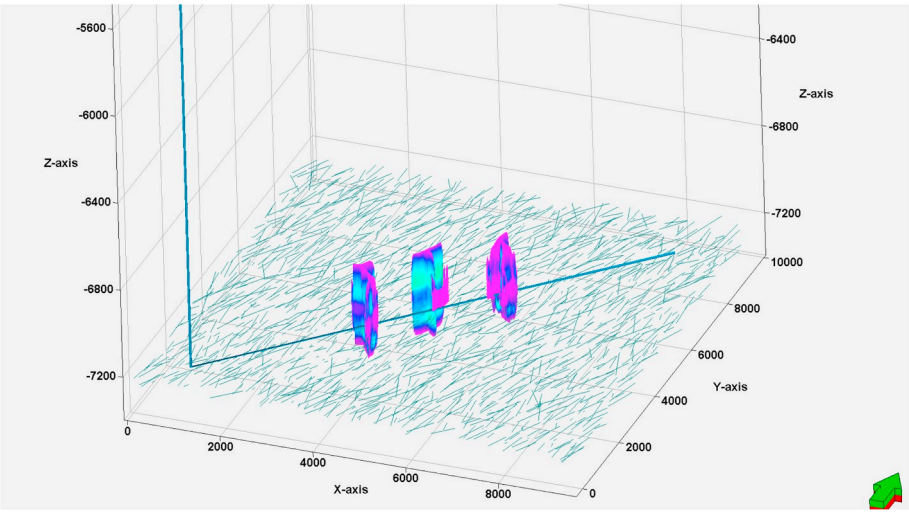

Fig. 14. Fracture geometry at the end of hydraulic fracturing operation under the proposed MPC.

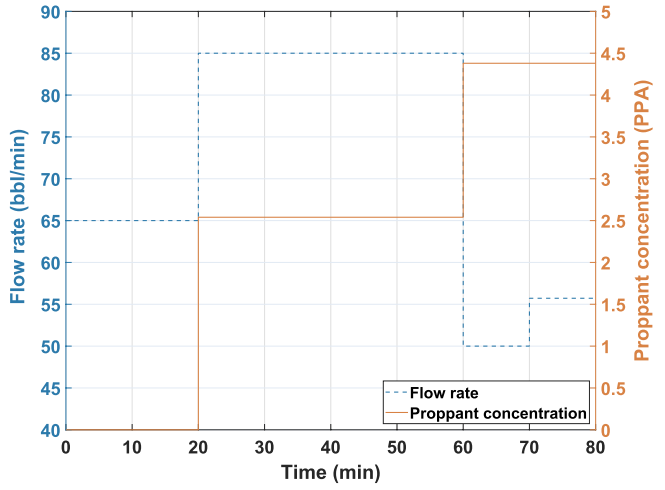

Fig. 15. Pumping schedule obtained under the proposed MPC.

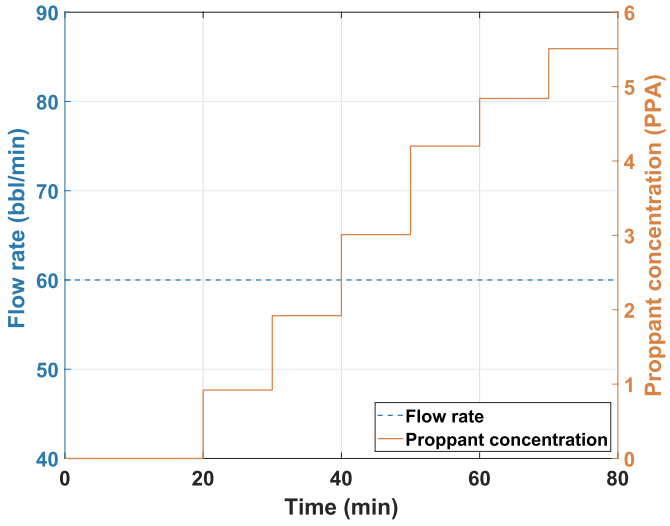

Fig. 16. Nolte's pumping schedule with input constraints being considered.

obtained by Siddhamshetty et al. (2019) and Nolte (1986), respectively.

Because linear ROMs were used to solve this problem, we achieved a significant reduction in the computational requirement. The time required to solve the optimization problem, Eq. (13), at every sampling time instant is given in Table 9. Since the problem was solved using a shrinking horizon approach, we can see that the computational time with every iteration has a tendency to decrease. Please note that all calculations were performed using MATLAB on a Dell workstation, powered by Intel(R) Core(TM) i7-4790 CPU@3.60GHz, running the Windows 8 operating system.

Natural fractures are present in most of unconventional reservoirs and affect hydraulic fracture propagation. Therefore, we cannot ignore the interaction of hydraulic fractures with natural fractures when we design pumping schedules to inject given fracturing resources. We have to utilize these interaction to achieve an even greater TFSA, which would not have been possible to achieve without considering natural fractures. Drainage area for hydrocarbon recovery is directly related to TFSA. Therefore, achieving a greater TFSA will lead to an increased oil production rate in naturally fractured unconventional reservoirs. The model-based pumping schedule design technique developed in this work considers the interaction of hydraulic fractures with natural fractures. Therefore, we were able to achieve a TFSA greater than those of the

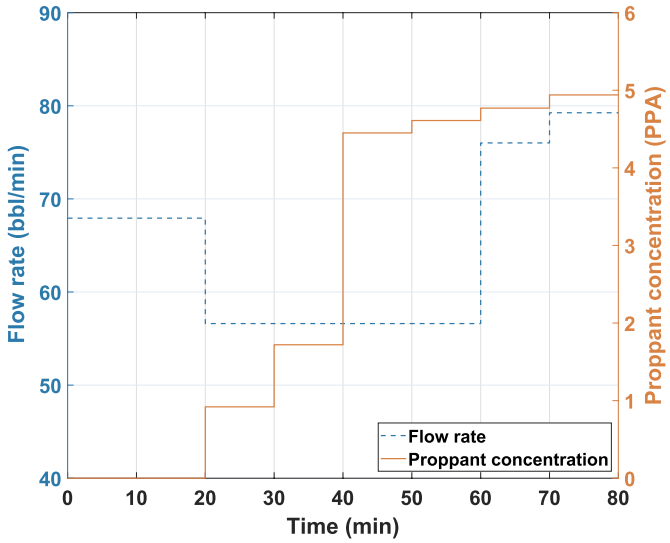

Fig. 17. Pumping schedule obtained by the method proposed by Siddhamshetty et al. (2019).

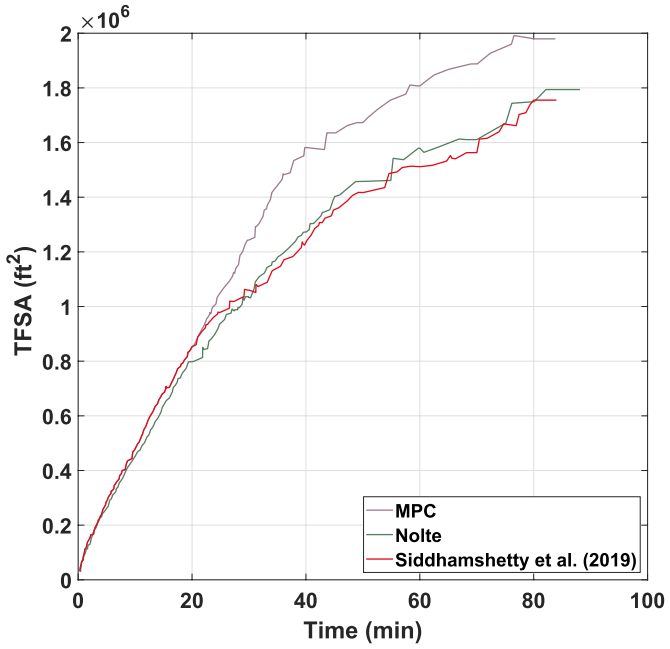

Fig. 18. Comparison of TFSA under the proposed MPC, Nolte's and Siddhamshetty et al. (2019) pumping schedules.

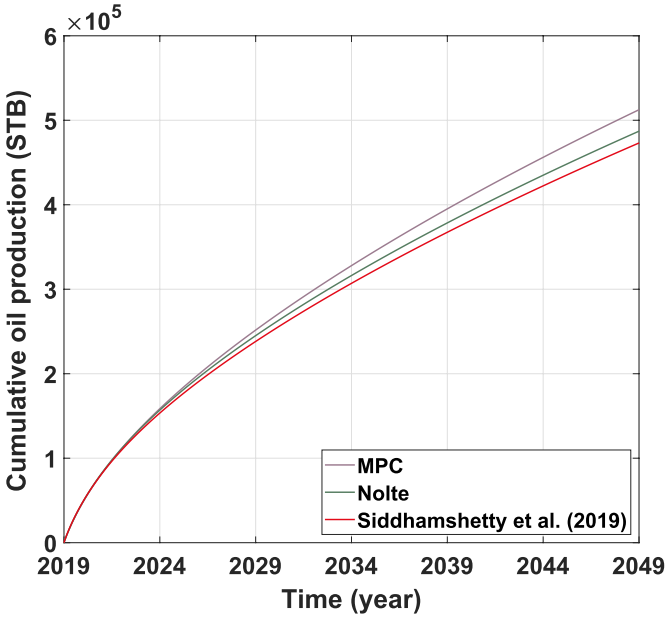

Fig. 19. Comparison of cumulative oil production under the proposed MPC, Nolte's and Siddhamshetty et al. (2019) pumping schedules.

existing pumping schedules which were developed without considering natural fractures.

8. Conclusions

In this work, it was observed from the sensitivity analysis that the cumulative oil production from a well is proportional to TFSA, which in-turn depends on the fracturing fluid pumping schedule for given fracturing resources and natural fracture distribution. Therefore, we developed a novel MPC framework to compute the fracturing fluid pumping schedule that maximizes TFSA in naturally fractured unconventional reservoirs. Initially, we constructed a ROM using the simulation data generated from Mangrove by considering the complex fracture growth in naturally fractured unconventional reservoirs. Then, the developed ROM was used for state estimation using a Kalman filter and available measurements. Next, a real-time MPC framework was developed utilizing the ROM and Kalman filter to compute the pumping schedule that maximizes TFSA. Simulation results presented in this work show that the maximum TFSA will lead to an oil production rate greater than those of the existing pumping schedules which were developed without considering natural fractures.

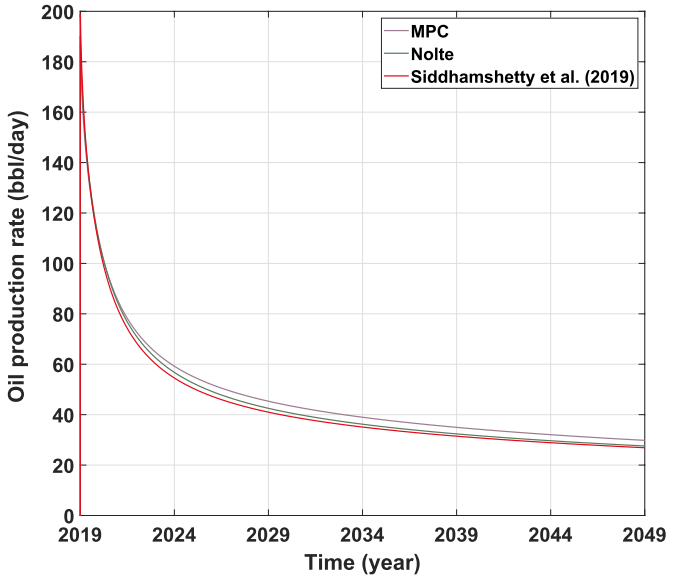

Fig. 20. Comparison of oil production rates under the proposed MPC, Nolte's and Siddhamshetty et al. (2019) pumping schedules.

Table 8
TFSA, cumulative oil production and NPV of oil produced under the proposed MPC, Nolte's and Siddhamshetty et al. (2019) pumping schedules.

	TFSA (ft^2)	Cumulative oil production (STB)	NPV (M
MPC	1979450	512707	13.36
Nolte	1793945	487310	12.96
Siddhamshetty et al. (2019)	1755249	473338	12.62

Table 9
Computational time required to solve the optimization problem, Eq. (13), at each pumping stage.

Pumping stage number	Computational time (s)
1	4.93
2	0.70
3	0.56
4	0.36
5	0.30
6	0.14
7	0.19
8	0.05

Acknowledgements

The authors gratefully acknowledge financial support from the National Science Foundation (CBET-1804407), the Texas A&M Energy Institute and the Artie McFerrin Department of Chemical Engineering.

References

Blanton, T., 1986. Propagation of hydraulically and dynamically induced fractures in naturally fractured reservoirs. In: SPE Unconventional Gas Technology Symposium (SPE 15261), Louisville, KY.

Budyn, E., Zi, G., Moes, N., Belytschko, T., 2004. A method for multiple crack growth in brittle materials without remeshing. Int. J. Numer. Methods Eng. 61, 1741–1770.

Chuprakov, D., Melchaeva, O., Prioul, R., 2013. Hydraulic fracture propagation across a weak discontinuity controlled by fluid injection. In: ISRM International Conference for Effective and Sustainable Hydraulic Fracturing (ISRM-ICHF-2013-008), Brisbane, Australia.

Chuprakov, D., Melchaeva, O., Prioul, R., 2014. Injection-sensitive mechanics of hydraulic fracture interaction with discontinuities. Rock Mech. Rock Eng. 47, 1625–1640.

Cipolla, C.L., Fitzpatrick, T., Williams, M.J., Ganguly, U.K., 2011. Seismic-to-simulation for unconventional reservoir development. In: SPE Reservoir Characterisation and Simulation Conference and Exhibition (SPE 146876), Abu Dhabi, UAE.

Crouch, S.L., Starfield, A.M., Rizzo, F.J., 1983. Boundary element methods in solid mechanics. J. Appl. Mech. 50, 704.

Dahi-Taleghani, A., Olson, J.E., 2009. Numerical modeling of multistranded hydraulic fracture propagation: accounting for the interaction between induced and natural fractures. In: SPE Annual Technical Conference Conference and Exhibition (SPE 124884), New Orleans, LA.

Dahi-Taleghani, A., Olson, J.E., 2013. How natural fractures could affect hydraulic-fracture geometry. SPE J. 19, 161–171.

Daniels, J.L., Waters, G.A., Le Calvez, J.H., Bentley, D., Lassek, J.T., 2007. Contacting more of the barnett shale through an integration of real-time microseismic monitoring, petrophysics, and hydraulic fracture design. In: SPE Annual Technical Conference and Exhibition (SPE 110562), Anaheim, CA.

Gale, J., Laubach, S., Olson, J., Eichhubl, P., Fall, A., 2014. Natural fractures in shale: a review and new observations. AAPG Bull. 98, 2165–2216.

Gale, J., Reed, R., Holder, J., 2007. Natural fractures in the Barnett Shale and their importance for hydraulic fracture treatments. AAPG Bull. 91, 603–622.

Gu, H., Weng, X., 2010. Criterion for fractures crossing frictional interfaces at non-orthogonal angles. In: 44th US Rock Mechanics Symposium and 5th US-Canada Rock Mechanics Symposium (ARMA-10-198), Salt Lake City, UT.

Gu, H., Weng, X., Lund, J.B., Mack, M.G., Ganguly, U., Suarez-Rivera, R., 2011. Hydraulic fracture crossing natural fracture at non-orthogonal angles, a criterion, its validation and applications. In: SPE Hydraulic Fracturing Technology Conference (SPE 139984), the Woodlands, TX.

Gu, Q., Hoo, K.A., 2014. Evaluating the performance of a fracturing treatment design. Ind. Eng. Chem. Res. 53, 10491–10503.

Gu, Q., Hoo, K.A., 2015. Model-based closed-loop control of the hydraulic fracturing process. Ind. Eng. Chem. Res. 54, 1585–1594.

Keshavarzi, R., Mohammadi, S., Bayesteh, H., 2012. Hydraulic fracture propagation in unconventional reservoirs: the role of natural fractures. In: 46th US Rock Mechanics/Geomechanics Symposium (ARMA-2012-129), Chicago, IL.

Mack, M.G., Elbel, J.L., Piggott, A.R., 1992. Numerical representation of multilayer hydraulic fracturing. In: The 33th US Symposium on Rock Mechanics (ARMA-92-0335), Santa Fe, NM.

Maxwell, S.C., Urbancic, T.I., Steinsberger, N., Zinno, R., 2002. Microseismic imaging of hydraulic fracture complexity in the barnett shale. In: SPE Annual Technical Conference and Exhibition (SPE 77440), San Antonio, TX.

Meyer, B.R., Bazan, L.W., 2011. A discrete fracture network model for hydraulically induced fractures-theory, parametric and case studies. In: SPE Hydraulic Fracturing Technology Conference (SPE 140514), the Woodlands, TX.

Narasingam, A., Siddhamshetty, P., Kwon, J.S., 2017. Temporal clustering for order reduction of nonlinear parabolic PDE systems with time-dependent spatial domains: application to a hydraulic fracturing process. AIChE J. 63, 3818–3831.

Narasingam, A., Siddhamshetty, P., Kwon, J.S., 2018. Handling spatial heterogeneity in reservoir parameters using proper orthogonal decomposition based ensemble kalman filter for model-based feedback control of hydraulic fracturing. Ind. Eng. Chem. Res. 57, 3977–3989.

Nolte, K.G., 1986. Determination of proppant and fluid schedules from fracturing-pressure decline. SPE Prod. Eng. 1, 255–265.

Olson, J.E., 2008. Multi-fracture propagation modeling: applications to hydraulic fracturing in shales and tight gas sands. In: The 42nd US Symposium on Rock Mechanics (ARMA-08-327), San Francisco, CA.

Olson, J.E., Taleghani, A.D., 2009. Modeling simultaneous growth of multiple hydraulic fractures and their interaction with natural fractures. In: SPE Hydraulic Fracturing Technology Conference (SPE 119739), the Woodlands, TX.

Renshaw, C., Pollard, D., 1995. An experimentally verified criterion for propagation across unbounded frictional interfaces in brittle, linear elastic materials. Int. J. Rock Mech. Min. Sci. Geomech. Abstr. 32, 237–249.

Scott, K.D., Chu, W.C., Flumerfelt, R.W., 2015. Application of real-time bottom-hole pressure to improve field development strategies in the midland basin wolfcamp shale. In: Unconventional Resources Technology Conference, San Antonio, TX, pp. 1790–1798.

Siddhamshetty, P., Kwon, J.S., 2019. Simultaneous measurement uncertainty reduction and proppant bank height control of hydraulic fracturing. Comput. Chem. Eng. 127, 272–281.

Siddhamshetty, P., Liu, S., Valkó, P.P., Kwon, J.S., 2017. Feedback control of proppant bank heights during hydraulic fracturing for enhanced productivity in shale formations. AIChE J. 64, 1638–1650.

Siddhamshetty, P., Wu, K., Kwon, J.S., 2018. Optimization of simultaneously propagating multiple fractures in hydraulic fracturing to achieve uniform growth using data-based model reduction. Chem. Eng. Res. Des. 136, 675–686.

Siddhamshetty, P., Wu, K., Kwon, J.S., 2019. Modeling and control of proppant distribution of multi-stage hydraulic fracturing in horizontal shale wells. Ind. Eng. Chem. Res. 58, 3159–3169.

Siddhamshetty, P., Yang, S., Kwon, J.S., 2018. Modeling of hydraulic fracturing and designing of online pumping schedules to achieve uniform proppant concentration in conventional oil reservoirs. Comput. Chem. Eng. 114, 306–317.

Sidhu, H.S., Narasingam, A., Siddhamshetty, P., Kwon, J.S., 2018. Model order reduction of nonlinear parabolic PDE systems with moving boundaries using sparse proper orthogonal decomposition: application to hydraulic fracturing. Comput. Chem. Eng. 112, 92–100.

Sidhu, H.S., Siddhamshetty, P., Kwon, J.S., 2018. Approximate dynamic programming based control of proppant concentration in hydraulic fracturing. Mathematics 6, 132.

Sukkar, Y.K., Cornell, D., 1955. Direct calculation of bottom-hole pressures in natural gas wells. Soc. Pet. Eng. 204, 43–48.

Sun, Z., Gu, Q., Dykstra, J., 2016. Uncertainty reduction of hydraulic fracturing process. In: American Control Conference (ACC), pp. 2135–2141.

Valko, P., Economides, M.J., 1995. Hydraulic Fracture Mechanics. Wiley, Chichester.

Wang, W., Olson, J.E., Prodanovic, M., 2013. Natural and hydraulic fracture interaction study based on semi-circular bending experiments. In: Unconventional Resources Technology Conference (SPE 168714), Denver, CO.

Warpinski, N., Teufel, L., 1987. Influence of geologic discontinuities on hydraulic fracture propagation. J. Pet. Technol. 39, 209–220.

Warpinski, N.R., Griffin, L.G., Davis, E.J., Grant, T., 2006. Improving hydraulic fracture diagnostics by joint inversion of downhole microseismic and tiltmeter data. In: SPE Annual Technical Conference and Exhibition (SPE 102690), San Antonio, TX.

Weng, X., Kresse, O., Chuprakov, D., Cohen, C.E., Prioul, R., Ganguly, U., 2014. Applying complex fracture model and integrated workflow in unconventional reservoirs. J. Pet. Sci. Eng. 124, 468–483.

Weng, X., Kresse, O., Cohen, C.E., Wu, R., Gu, H., 2011. Modeling of hydraulic fracture network propagation in a naturally fractured formation. In: SPE Hydraulic Fracturing Technology Conference (SPE 140253), the Woodlands, TX.

Wu, K., Olson, J., 2014. Mechanics analysis of interaction between hydraulic and natural fractures in shale reservoirs. In: Unconventional Resources Technology Conference, Denver, CO, pp. 1824–1841.

Wu, K., Olson, J.E., 2016. Numerical investigation of complex hydraulic-fracture development in naturally fractured reservoirs. SPE Prod. Oper. 31, 300–309.

Xu, W., Le Calvez, J.H., Thiercelin, M.J., 2009. Characterization of hydraulically-induced fracture network using treatment and microseismic data in a tight-gas sand formation: a geomechanical approach. In: SPE Tight Gas Completions Conference (SPE 125237), San Antonio, TX.

Xu, W., Thiercelin, M.J., Ganguly, U., Weng, X., Gu, H., Onda, H., Sun, J., Le Calvez, J., 2010. Wiremesh: a novel shale fracturing simulator. In: International Oil and Gas Conference and Exhibition in China (SPE 132218), Beijing, China.

Yang, R., Huang, Z., Yu, W., Li, G., Ren, W., Zuo, L., Tan, X., Sepehrnoori, K., Tian, S., Sheng, M., 2016. A comprehensive model for real gas transport in shale formations with complex non-planar fracture networks. Sci. Rep. 6, 36673.

Yang, S., Siddhamshetty, P., Kwon, J.S., 2017. Optimal pumping schedule design to achieve a uniform proppant concentration level in hydraulic fracturing. Comput. Chem. Eng. 101, 138–147.